Check for updates

Stratospheric intrusion may aggravate widespread ozone pollution through both vertical and horizontal advections in eastern China during summer

Fengyi Chang, Jiandong Li, Nan Li* and Hong Liao*

Jiangsu Key Laboratory of Atmospheric Environment Monitoring and Pollution Control, Jiangsu Collaborative Innovation Center of Atmospheric Environment and Equipment Technology, School of Environmental Science and Engineering, Nanjing University of Information Science and Technology, Nanjing, China

Stratospheric intrusion (SI) is an important source of tropospheric ozone (O_3). Here, we used the online coupled Weather Research and Forecasting-Chemistry (WRF-Chem) model to simulate a typical SI event that occurred over eastern China on 15–19 July 2016 and investigate the impacts of SI on near-surface O_3 pollution. The results show that the large-scale circulation of SI was characterized by a deep trough over central China and South Asia high and Western Pacific Subtropical high located to the east and west of the deep trough, respectively. With the evolution of the deep trough, the strong downdrafts behind the trough lead to O_3-rich air injected into the lower troposphere across eastern China. By using a tracer tagging method in WRF-Chem, we quantified the SI contributed up to 6.5 ppb to the surface O_3 concentration. According to the integrated process rate analyses, which were employed to quantify the contribution of different physical/chemical processes to O_3, the advection process dominated variations in troposphere O_3 with positive contribution ranging from 0.1 to 13.8 ppb h^{-1}. As altitude decreases, the contribution of advection diminishes as the intensity of the SI gradually weakens. Although the vertical advection contributed limited O_3 that directly reached the ground, we revealed that the SI has significant impact on near-surface O_3 over a large territory of eastern China through regional transport by horizontal advection process. Below 691 m, the positive contribution of horizontal advection to O_3 ranges from 1.6 to 13.4 ppb h^{-1}. This study highlights the natural effect of SI on summertime O_3 pollution in eastern China and will help the development of a future O_3 pollution alert system.

KEYWORDS

ozone, stratospheric intrusion, eastern China, IPR (integrated process rate), WRF-Chem

1 Introduction

High concentrations of surface ozone (O_3) are detrimental to human health (Lelieveld et al., 2015; Fleming et al., 2018; Xu et al., 2020) and crop yields (Mills et al., 2018). O_3 pollution has increased recently in China, surpassing $PM_{2.5}$ as a major pollutant that deteriorates urban air quality (Li et al., 2019a; Li et al., 2019b; Zhai et al., 2019; Li et al., 2020). Near-surface O_3 is produced *via* photochemical reactions involving nitrogen oxides and volatile organic compounds (Finlayson-Pitts, 1997; Wang et al., 2017). In addition to anthropogenic and biogenic emissions, stratospheric intrusion (SI), which is characterized

TABLE 1 Parameterizations used in the WRF-Chem model.

Options	WRF-chem
Microphysics option	Purdue Lin scheme
Longwave radiation option	RRTMG scheme
Shortwave radiation option	RRTMG scheme
Photolysis scheme	Fast-J
Chemistry option	SAPRC99
Aerosol option	MOSAIC
Boundary layer option	YSU scheme
Cumulus option	Grell 3-Densemble scheme

by O_3-rich air in the mid-troposphere with high potential vorticity (PV) and low relative humidity (RH) (Ganguly, 2012; Greenslade et al., 2017), can contribute to elevated O_3 concentrations (Davies and Schuepbach, 1994; Stohl et al., 2003a). Such a natural process complicates the development of emission-reduction strategies. The dynamical mechanism underlying SI are complex. Previous studies have revealed that SI are mainly related to weather processes such as cut-off lows and tropopause folding (Langford et al., 1996; Nieto et al., 2005; Li et al., 2015; Chen et al., 2021).

Direct observation of O_3 pollution caused by SI is challenging because of the large dynamic variability of the tropopause and the lack of high-resolution spatial and temporal measurements. Hocking et al. (2007) detected stratospheric O_3 intrusion events using wind profiler radar and illustrated that wind profile data could be used to predict the probability of O_3 intrusion. By using the MERRA-2 reanalysis in combination with surface O_3 and satellite observations and GEOS-5 simulated carbon monoxide and a stratospheric tracer, Knowland et al. (2017) found that SI events are associated with the tropopause folding under the jet stream and subsequent isentropic descent of dry, O_3-rich stratospheric air toward the surface. Huang et al. (2022) used Be[7] as a tracer for stratosphere–troposphere exchange to diagnose SI events. Ou-Yang et al. (2022) use thresholds for surface O_3, carbon monoxide, and RH to detect SI episodes at Lulin Atmospheric Background Station, a high-altitude site in East Asia.

SIs have also been extensively investigated in modelling studies. Based on the GFDL AM3 model, Lin et al. (2015) highlighted that SI can frequently occur during spring when the polar jet stream is abnormally contorted to conflict with the attainment of the national ambient air quality standard at high-elevation western US regions. Through the use of the ECHAM5/MESSy Atmospheric Chemistry model simulations, Akritidis et al. (2016) found a high correlation between interannual variability of near-surface O_3 and tropopause folding in the Eastern Mediterranean. During selected intrusion events, the air masses moved in a southeasterly direction. Using WACCM6 model simulations, Wang X. et al. (2020) found a significant 18% average contribution of SI to O_3 extreme events in the western United States. The weather research and forecasting coupled with chemistry (WRF-Chem) was utilized by Zhao et al. (2021a) to investigate a SI that occurred in Hong Kong in spring. They found that the subtropical high-level jet stream was the primary driver of this SI. Zhao et al. (2021b) used the process analysis technique in WRF-Chem

to examine the occurrence of SI and concluded that vertical advection is the predominant cause of the increase in O_3 in the lower troposphere. Based on observations and model simulation, Zhang et al. (2022) estimated the mean magnitude of SI contribution was 1.5–10 ppb in the North China Plain. Meng et al. (2022) used reanalysis data, observations and LaGrange models to investigated the effect of SI on summer O_3 in the North China Plain. The results showed that the contribution of SI to surface O_3 was estimated to be 5.7%–18.8% and it is closely related to the high-altitude westerly circulation over the Asian region. These findings suggested an important role of SI in O_3 enhancement episodes, and more observations are needed to properly constrain and quantify its impacts.

Eastern China is one of the most developed regions in China and has become an economic center in recent years. However, the fast economic development also resulted in a substantial rise in air pollutant emissions, leading to severe photochemical pollution (Dang and Liao, 2019; Tang et al., 2022). Some studies have revealed transportation can induce O_3 pollution in the eastern China (Gong et al., 2020; Dai et al., 2021; Dang et al., 2021; Qian et al., 2022), but few have linked wide-spread transportation to SI. Here we used air quality observations and the WRF-Chem model to simulate a SI event in eastern China in summer and explore its dynamical processes. The integrated process analysis was used to quantify the contribution of SI to surface O_3 concentration.
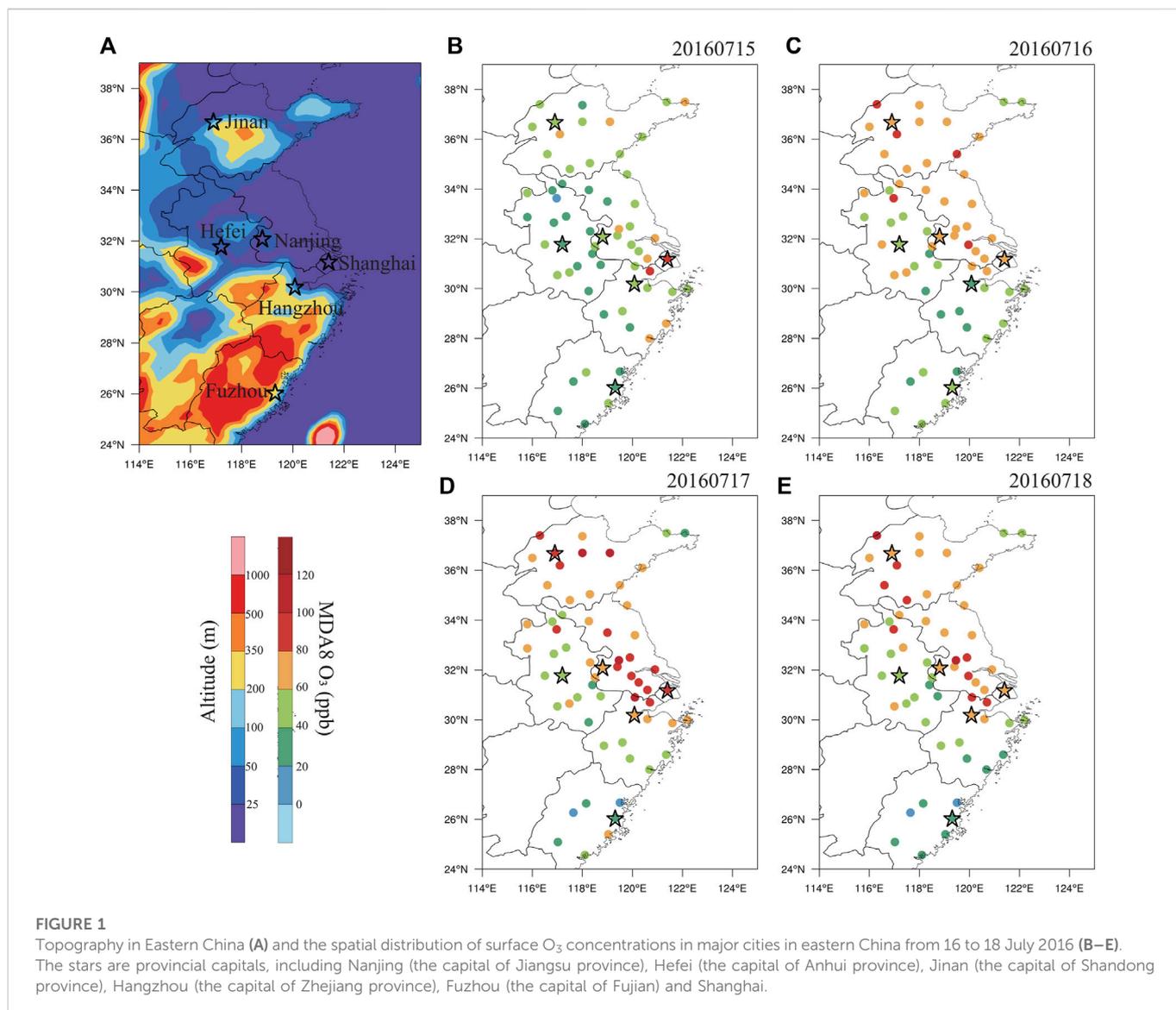
2 Data and methods

2.1 Observational data

Near-surface O_3 observations were obtained from the China National Environmental Monitoring Center (CNEMC, http://106.37.208.233:20035/). The days with maximum daily 8-h average (MDA8) O_3 concentrations exceeding 82 ppb were defined as O_3 pollution episodes based on the National Ambient Air Quality Standard (GB 3095–2012) Grade II issued by the Ministry of Ecology and Environment of China. Surface meteorological observations, including temperature, RH and wind vectors are downloaded from http://www.Meteomanz.com/.

2.2 Model configurations

WRF-Chem (v3.9.1) is an open-source regional chemical transport model developed by the US National Center for Atmospheric Research (NCAR). WRF-Chem is capable of simulating air quality with fully coupled meteorology and chemistry (Grell et al., 2005). Initial and boundary meteorological conditions were derived from FNL reanalysis data (https://rda.ucar.edu/datasets/ds083.2/) by the National Centers for Environmental Prediction (NCEP). The anthropogenic emissions were obtained from the Multi-resolution Emission Inventory for China (MEIC, http://meicmodel.org/), which was developed by Tsinghua University (Li et al., 2017). Online biogenic and real-time biomass burning emissions were calculated from the Model of Emissions of Gases and Aerosols from Nature (MEGAN, v2.1) tool (A. Guenther et al.,

FIGURE 1
Topography in Eastern China **(A)** and the spatial distribution of surface O$_3$ concentrations in major cities in eastern China from 16 to 18 July 2016 **(B−E)**. The stars are provincial capitals, including Nanjing (the capital of Jiangsu province), Hefei (the capital of Anhui province), Jinan (the capital of Shandong province), Hangzhou (the capital of Zhejiang province), Fuzhou (the capital of Fujian) and Shanghai.

2006) and Fire INventory from NCAR (FINN, https://www2.acom.ucar.edu/modeling/finn-fire-inventory-ncar) (Wiedinmyer et al., 2011) respectively. The initial and boundary conditions of chemical specials were provided by the global chemical transport model MOZART (L. K. Emmons et al., 2010). Meanwhile, the Statewide Air Pollution Research Center (SAPRC99) mechanism was utilized for the gas phase reaction scheme in our study (Carter, 2000). For aerosols, we applied the Model for Simulating Aerosol Interactions and Chemistry (MOSAIC) as the aerosol parameterization (Zaveri et al., 2008).

Following Barth et al. (2012), we added the upper boundary condition scheme to overcome WRF-Chem's inability to simulate O$_3$ in the stratosphere. This scheme adjusts key chemical species (i.e., O$_3$, nitrogen oxides, nitric acid, methane, monoxide carbon, Nitrous Oxide, nitrogen oxide) concentrations to climatological averages based on the out of a global atmospheric chemical model. The idealized chemical profile from 50 hPa down to the tropopause are replaced with these values. The temperature from WACCM is

used to calculate tropopause height, which subsequently serves as the upper boundary condition in WRF-Chem (Barth et al., 2012; Lamarque et al., 2012). This upper boundary condition scheme will enable WRF-Chem to accurately simulate the stratosphere-troposphere exchanges and quantify the impact of SI on the concentration of chemical species in the troposphere.

The simulation ran from July 13 to 19 July 2016, with the first 48 h saved as the spin-up period. The WRF-Chem domain covers the whole of China, with a horizontal resolution of 27 × 27 km and 43 vertical layers from the surface to 50 hPa. Table 1 presented the physical parameterization for subgrid processes, such as radiation, microphysics, and the surface layer.

2.3 Statistical methods for comparisons

To statistically quantify the model performance, we used three indicators, i.e., the index of agreement (IOA), the normalized

TABLE 2 Model performance in predicting meteorological parameters over cities during the study period. The T, WS, WD, and RH represent temperature, wind speed, wind direction and relative humidity, respectively.

Cities		Observation	Simulation	IOA	NMB
Shanghai	T (°C)	28.7	26.5	0.73	−7.8%
	WS (m/s)	2.37	2.62	0.57	11.0%
	WD	159.7	190.8	0.73	19.4%
	RH (%)	77.8	87.2	0.69	12.1%
Nanjing	T (°C)	27.6	26.5	0.82	−4.1%
	WS (m/s)	2.54	2.48	0.65	−2.3%
	WD	175.8	186.7	0.74	6.16%
	RH (%)	79.7	86.5	0.70	8.4%
Hefei	T (°C)	27.0	24.6	0.68	−9.1%
	WS (m/s)	3.23	3.43	0.61	6.2%
	WD	173.2	187.9	0.67	8.51%
	RH (%)	83.1	87.8	0.69	5.8%
Hangzhou	T (°C)	29.1	26.5	0.70	−9.1%
	WS (m/s)	2.14	2.88	0.69	34.6%
	WD	170.1	189.6	0.71	11.5%
	RH (%)	78.3	86.7	0.70	10.8%
Jinan	T (°C)	24.7	25.7	0.76	4.5%
	WS (m/s)	3.41	4.79	0.81	40.5%
	WD	145.9	125.3	0.57	−14.1%
	RH (%)	79	76.5	0.70	−3.1%
Fuzhou	T (°C)	28.4	27.7	0.76	−2.6%
	WS (m/s)	3.63	4.09	0.76	12.4%
	WD	207.1	194.6	0.72	−6.0%
	RH (%)	80.5	87.8	0.74	8.9%

mean bias (NMB) and the correlation coefficient R). IOA measures the degree of agreement between the model and observations and ranges from 0 to 1, with one indicating perfect agreement. The sign of NMB reveals whether the modeled mean underestimates or overestimates the observed mean, whilethe values of NMB indicates the magnitude of the underestimation or overestimation (Jr and Yu, 2012). Generally, model performance is excellent if NMB is close to 0. R describes the degree of association between two variables (Asuero et al., 2007). In model studies, R greater than 0.7 between simulations and observations is considered to be a good correlation.

$$IOA = 1 - \frac{\sum_{i=1}^{N}(SIM_i - OBS_i)^2}{\sum_{i=1}^{N}\left(\left|SIM_i - \overline{SIM}\right| + \left|OBS_i - \overline{OBS}\right|\right)^2} \quad (1)$$

$$NMB = \frac{\sum_{i=1}^{N}(SIM_i - OBS_i)}{\sum_{i=1}^{N}OBS_i} \quad (2)$$

$$R = \frac{\sum_{i=1}^{N}\left|(OBS_i - \overline{OBS_i}) \cdot (SIM_i - \overline{SIM_i})\right|}{\sqrt{\sum_{i=1}^{N}(OBS_i - \overline{OBS_i})^2 + \sum_{i=1}^{N}(SIM_i - \overline{SIM_i})^2}} \quad (3)$$

where SIM_i, OBS_i, are the hourly observed and simulated data and N is the total number of hours, and $\overline{OBS}$ and $\overline{SIM}$ represent the averages of observations and model results, respectively.

2.4 Tracer method

To track stratospheric air, one tracer was included. In the WRF-Chem, the stratospheric tracer is defined as a value of one from the
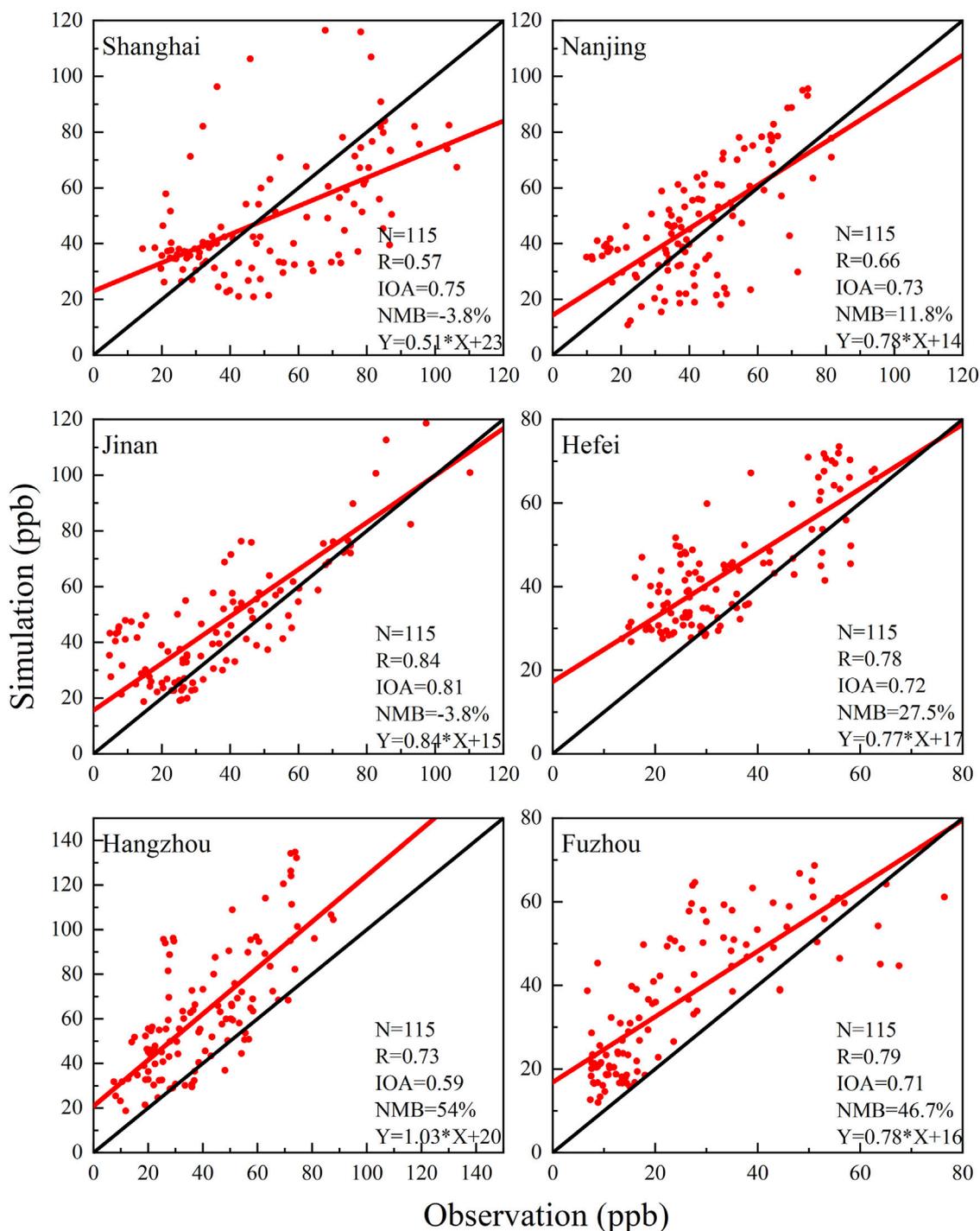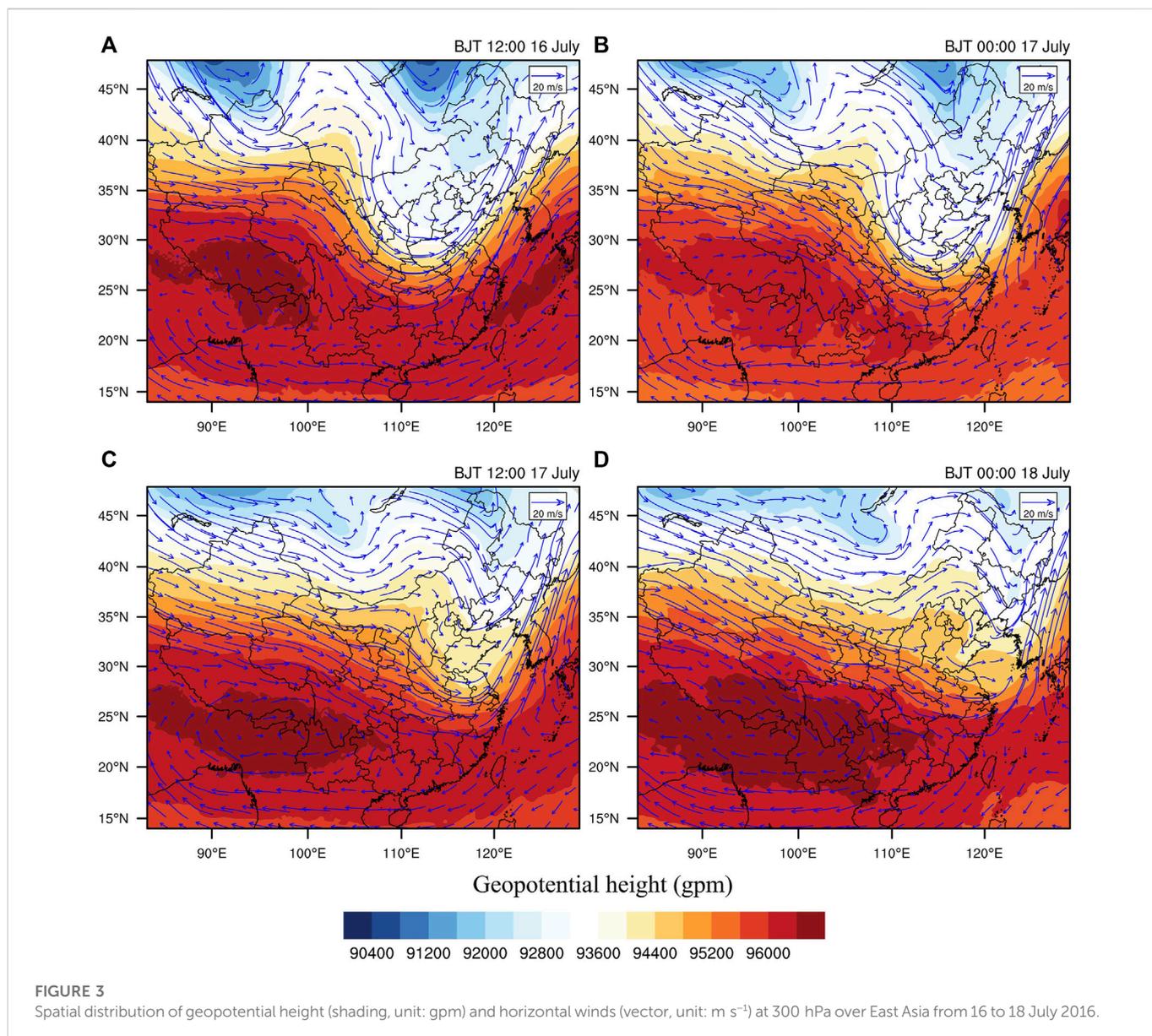
FIGURE 2
Scatter plots of O_3 between simulations and observations for the six provincial capitals in eastern China. The IOA, NMB, R represent the index of agreement, the normalized mean bias and the correlation coefficient, respectively, N denotes the total number of hours.

height of the tropopause to the top of the model. The stratospheric tracer in the model was physically transported during the WRF-Chem simulation. The stratospheric O_3 (O_3S) is calculated by multiplying the stratospheric tracer by the tropopause O_3 concentration. The percentage of stratospheric O_3 (O_3P) is calculated by the ratio of O_3S and surface O_3 concentration (Barth et al., 2012; Ni et al., 2019).

2.5 Integrated process rate analysis

The integrated process rate (IPR) analysis has been widely used to quantify the contributions of different processes to O_3 variations (Gonçalves et al., 2009; Gao et al., 2016; Gao et al., 2018). In this study, five processes are considered, including vertical mixing

FIGURE 3
Spatial distribution of geopotential height (shading, unit: gpm) and horizontal winds (vector, unit: m s^{-1}) at 300 hPa over East Asia from 16 to 18 July 2016.

(VMIX), sub-grid convection (CONV), net chemical production (CHEM), horizontal advection (ADVH), and vertical advection (ADVZ). VMIX is initiated by turbulence and is closely associated with the development of planetary boundary layer (PBL), which influences O$_3$ vertical diffusion. CHEM represents the net O$_3$ chemical production (production minus consumption). ADVH and ADVZ indicate transport by winds (Gao et al., 2016; Ou-Yang et al., 2022). ADV is defined as the sum of ADVH and ADVZ. NET is the sum of all physical and chemical processes that contribute to variations in O$_3$ concentrations.

3 Result and discussion

3.1 Model evaluation

We focused on a SI event that occurred in eastern China on 16–18 July 2016. Figure 1 shows the spatial distribution of maximum daily 8-h average (MDA8) O$_3$ concentrations for cities in eastern China during the SI event from 15 to 18 July. The air quality was generally clean with MDA8 O$_3$ concentrations being lower than 60 ppb on 15 July. Then, the pollution episode began to develop with MDA8 O$_3$ concentrations ranging between 60 and 80 ppb in Jiangsu and Shandong. The MDA8 O$_3$ concentrations even reached 100 ppb on July 17, exceeding the MDA8 O$_3$ national air quality grade II standard of 82 ppb (equal to 160 ug m^{-3} at 298 K and 1,013 hPa. The O$_3$ pollution episode was gradually mitigated on July 18. We employed the WRF-Chem model to examine the contribution of SI to near-surface O$_3$ during this widespread pollution.

First, we evaluated the performance of the model in simulating meteorological parameters, including temperature, RH, wind speed and wind direction (Table 2). Generally, the model simulated well in reproducing temporal variations in meteorological parameters in eastern China, with IOA values ranging between 0.57 and 0.81. The simulated temperature and RH agreed well with observations,
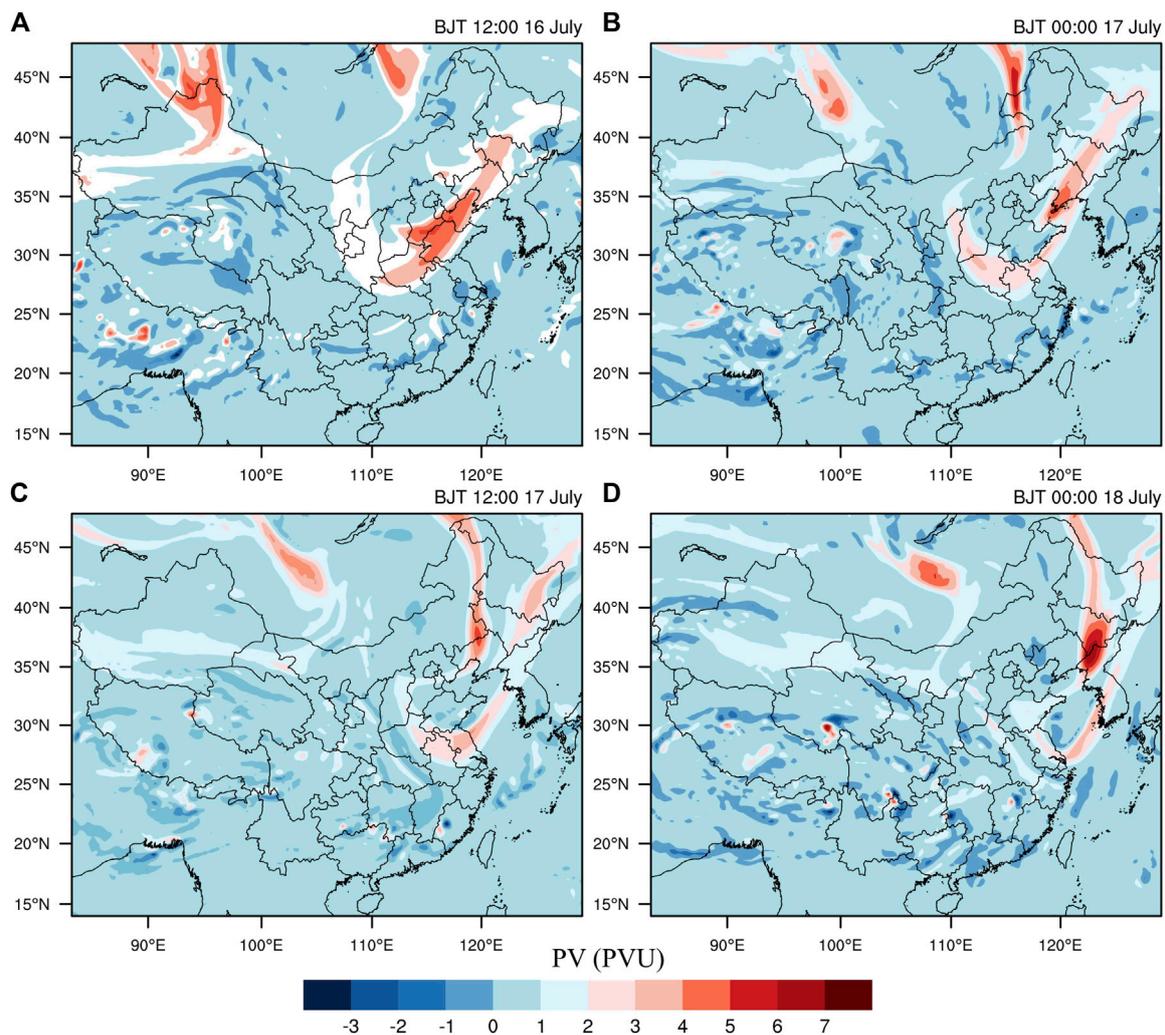
FIGURE 4
Spatial distribution of potential vorticity (PV, unit: 10^{-6} m² K s⁻¹ kg⁻¹) at 300 hPa over East Asia from 16 to 18 July 2016.

with absolute NMB lower than 12%. For wind speed, we found high NMB for Hangzhou (34.6%) and Jinan (40.5%), which may due to the unresolved topographic features in the surface drag parameterization and the coarse resolution (Yahya et al., 2015; Zhang et al., 2015; Chen et al., 2019). The IOA values were in the range of 0.57–0.74 and the absolute NMB values were in the range of 6.0%–19.4%, indicating that the WRF-Chem model captured wind direction fairly well.

Figure 2 shows the scatter plots of simulated *versus* observed hourly O_3 concentrations and their regression statistics for six provincial capitals (Shanghai, Nanjing, Hangzhou, Fuzhou, Jinan, and Hefei) in eastern China. The mean IOA, R and regression slope is 0.72, 0.73 and 0.78, respectively, indicating a good agreement between simulation and observation. We also note that surface O_3 concentrations were overestimated by 11.8%–54.0%, which might result from the PBL parameterization scheme (YSU scheme) and boundary input from the MOZART-4 model. It was suggested that the YSU scheme overestimated the nighttime PBL, which increased nighttime surface O_3 by enhancing vertical mixing (Žabkar et al., 2011; Karlický et al., 2017). Abdallah et al. (2016) also found the

boundary conditions from the MOZART-4 model were responsible for the overestimation of O_3 in the *Polyphemus* chemical transport model. In addition, the model accuracy is also limited by the resolution (0.25° × 0.25°) of emission inventory (Gao et al., 2016). Despite these uncertainties, model simulations were capable of reproducing the spatial and temporal characteristics of O_3 and meteorological parameters during SI.

3.2 Weather conditions during stratosphere intrusion

Figure 3 shows the synoptic conditions during SI over East Asia in the upper troposphere (300 hPa). The large-scale circulation pattern was characterized by a deep trough over central-to-North China, the South Asia high and the Western Pacific subtropical high (Figure 3A). Two cold eddies located around 45–50°N in northern Xinjiang and Mongolia, respectively, continuously brought cold air to the deep trough. The deep trough was developed from 12:00 BJT on 16 July to its peak at 00:00 BJT on
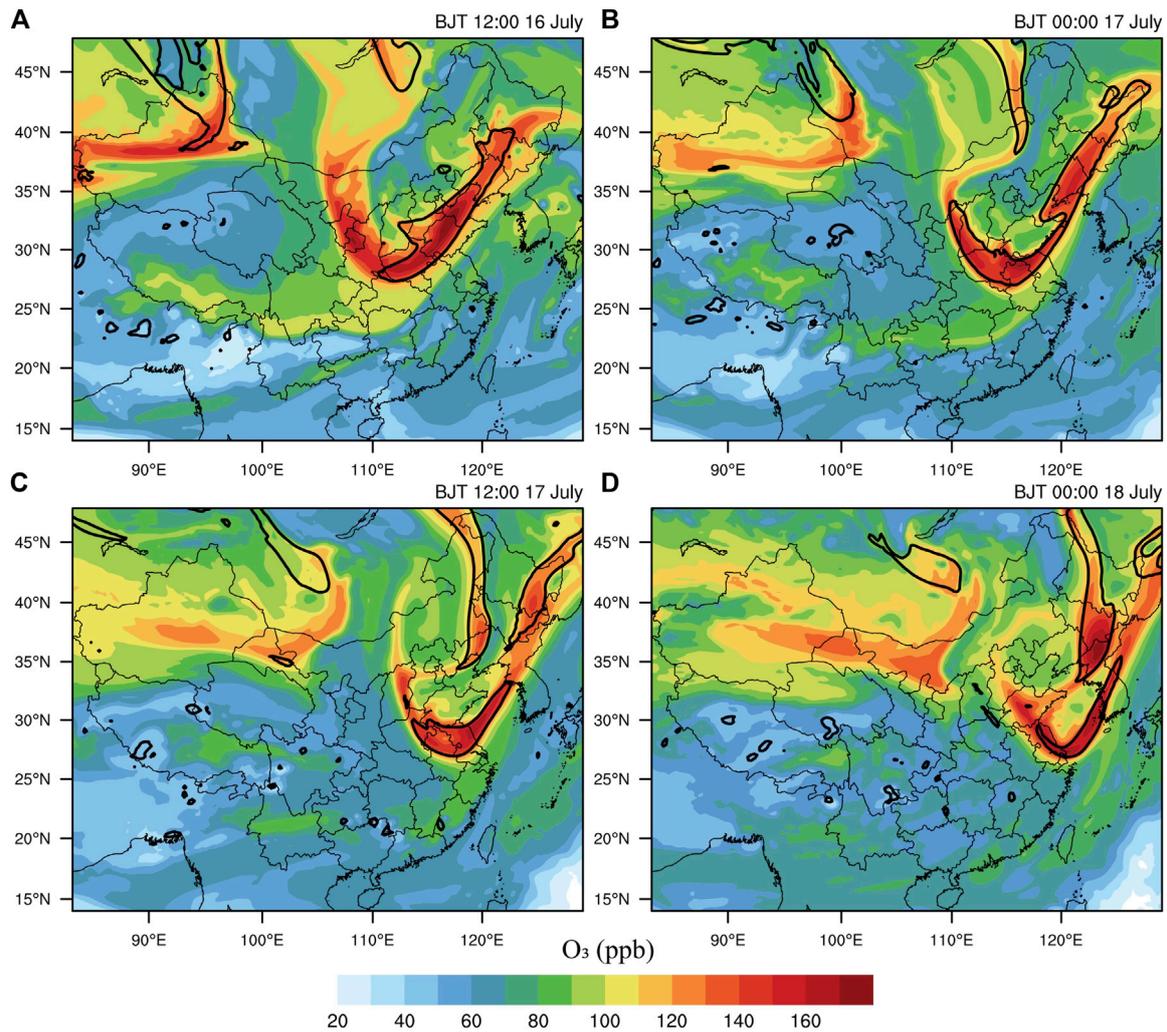
FIGURE 5
Spatial distribution of O$_3$ (unit: ppb) at 300 hPa over East Asia from 16 to 18 July 2016. The black contour line indicates the dynamical tropopause of 2 PVU
(1 PVU = 10^{-6} m^2 s^{-1} K kg^{-1}).

17 July, then gradually decayed at 00:00 BJT on 18 July. During the eastern development of the deep trough, the downdraft in the west of the upper-level trough were expected to carry O$_3$-rich stratospheric air into the troposphere across eastern China.

A PV of 2 PVU (10^{-6} m^2 K s^{-1} kg^{-1}) is referred to as a dynamical tropopause at the midlatitude (Holton et al., 1995; Stohl et al., 2003b). Elevated PV in the tropopause can be used as a marker to indicate stratosphere intrusion which may lead to enhanced O$_3$ concentration in the troposphere. Figure 4 shows the spatial distribution of PV at 300 hPa. We see that the regions with PV exceeding 2 PVU coincided with the passage of the deep trough shown in Figure 3. On 16 July (Figure 4A), high PV values were identified over northern Xinjiang, eastern Mongolia and northern China, corresponding to the three upper-level troughs in Figure 3A. Along with the development of the deep trough in central China, high PV values were found over eastern China on 17 July, indicating the SI occurred there.

3.3 The impact of stratospheric intrusion on tropospheric O$_3$

Figure 5 shows the spatial distribution of O$_3$ at 300 hPa from 16 to 18 July 2016. The simulated O$_3$-rich stratospheric air match well with the high-PV regions. At 12:00 BJT on 16 July, the O$_3$ concentration in eastern China was about 80–120 ppb, and the O$_3$ tongue exceeding 110 ppb moved to 116° E after 12 h. As the deep trough moved eastward, the maximum center was identified at Jiangsu and Shandong provinces at 12:00 BJT on 17 July, with high O$_3$ concentration that exceeded 150 ppb (Figure 5C). Based on the former analysis, the high-O$_3$ concentrations at 300 hPa were attributed to the downward transport of O$_3$ from the stratosphere during SI.

In order to study the depth of SI, the longitude-pressure cross-section of WRF-Chem simulated O$_3$ and PV along the latitude of 30°–34°N were shown in Figure 6. Tongue plumes with O$_3$ concentrations exceeding 160 ppb extend from 100 hPa to
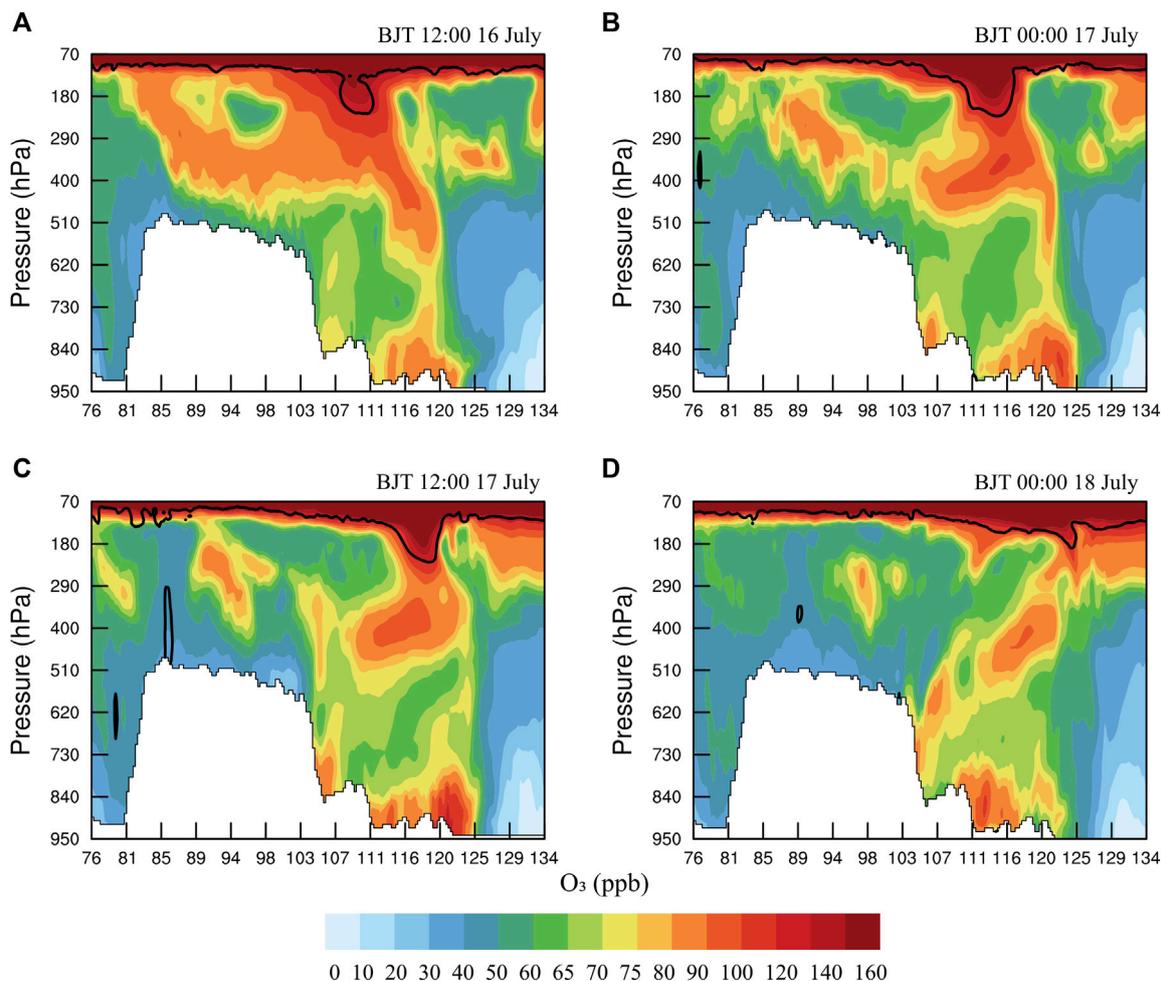
FIGURE 6
Longitude-pressure cross-section of WRF-Chem simulated O_3 (unit: ppb) averaged over the longitude of 30°–34°N from 16 to 18 July 2016. The black contour line indicates the dynamical tropopause of 2 PVU.
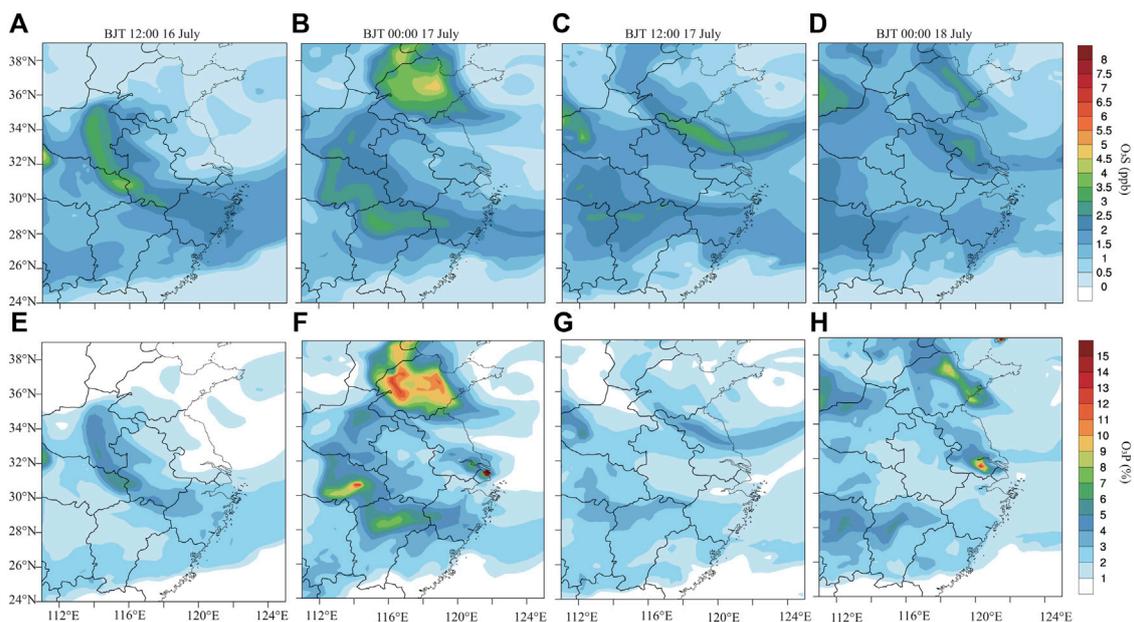

FIGURE 7
Spatial distribution of surface O_3S and O_3P in eastern China from 16 to 18 July 2016.
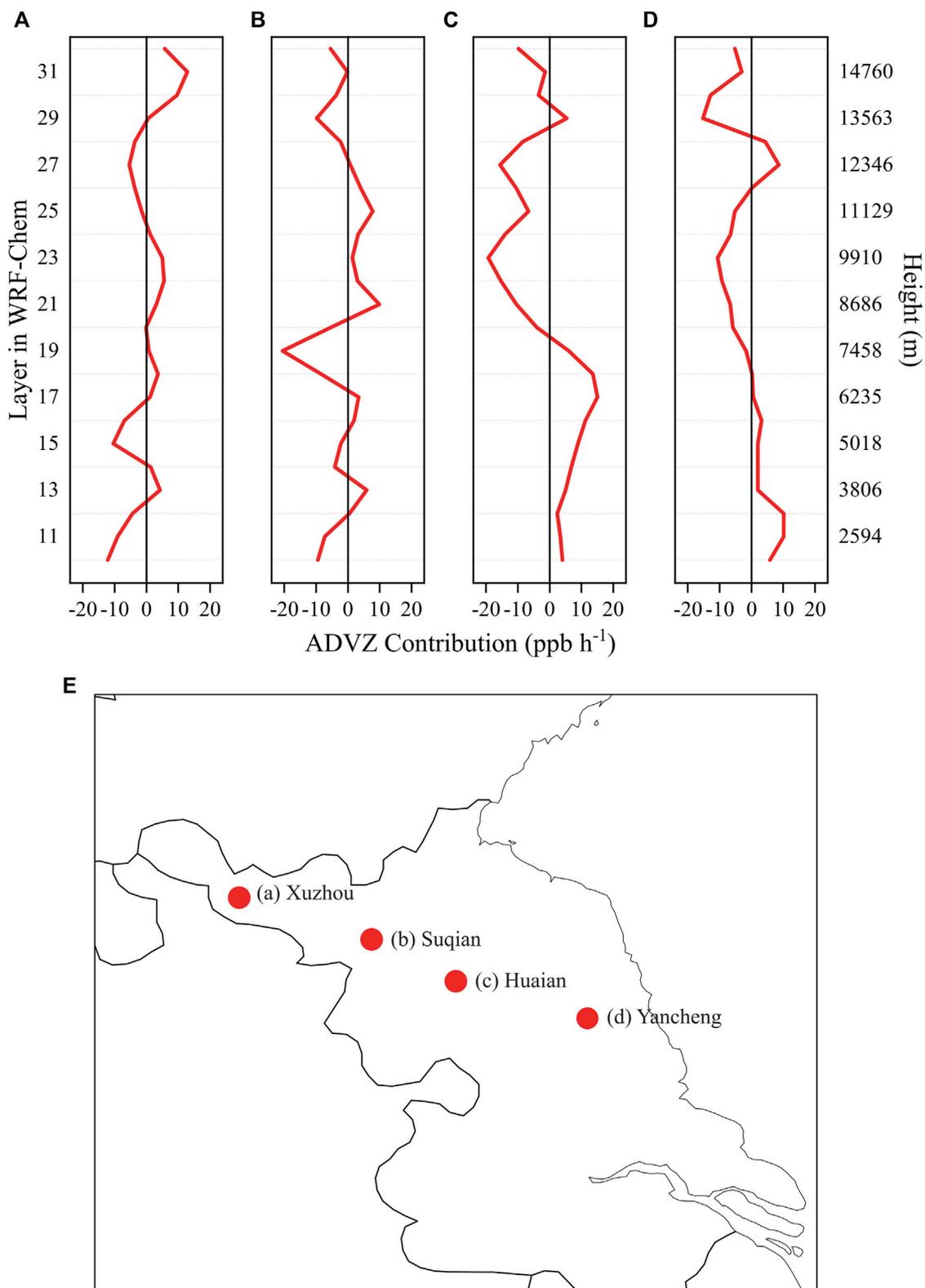
FIGURE 8
Vertical profiles of the ADVZ contributions **(A–D)** from four grid points in the northwest direction over Jiangsu province **(E)** during the intrusion.

280 hPa, representing the downward transport of stratospheric O_3. This tongue-like plume moved from 110° E to 118° E with the development of the upper-level trough. At 12:00 BJT on 16 July, a band of high O_3 concentration of 70–140 ppb extended from the top of the troposphere to near 800 hPa over eastern China (116°–120°E). Note that not every SI event can influence the
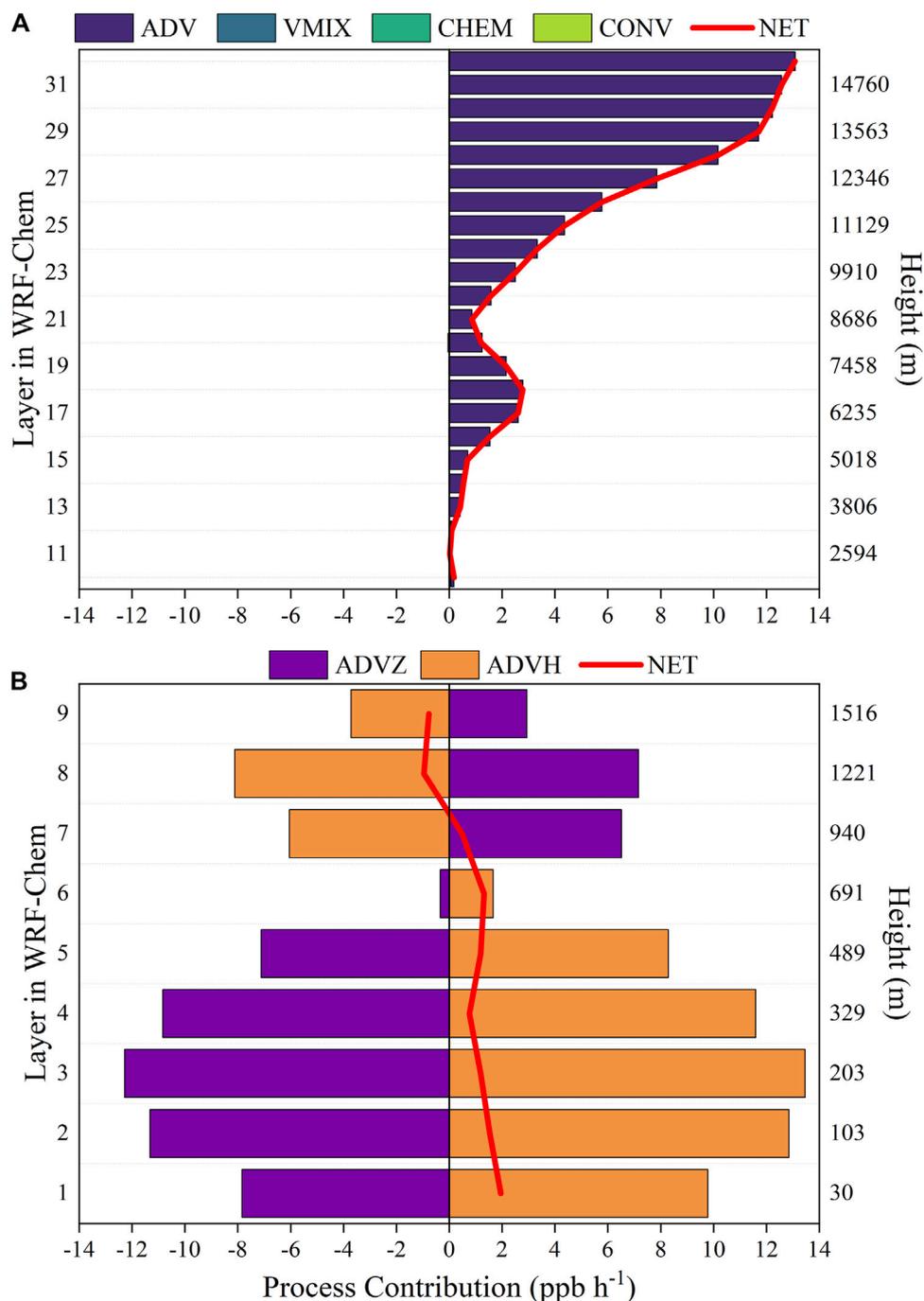
FIGURE 9
Changes in O_3 during the stratospheric intrusion. The red lines denote the net contribution of all processes (NET; defined as ADV + VMIX + CHEM).

near-surface O_3. For example, Wang H. et al. (2020) identified a SI on 11–12 July 2016 over eastern China, and suggested that the SI did not reach the ground.

To further confirm the impact of SI on surface O_3, we investigated the stratosphere O_3 tracers following the method in Section 2.4. Figure 7 shows the spatial distribution of O_3S and O_3P at the surface from 16 to 18 July 2016. The O_3S values in Jiangsu and Shandong provinces were very low at 12:00 BJT on July 16. After 12 h, the maximum value of O_3S reached 6 ppb (Figure 7B). The larger O_3S values cover almost the whole of Shandong province. At 12:00 BJT on

July 17, the maximum center of O_3S moved to Jiangsu province with values of 2–4 ppb. We then calculated the relative stratospheric contribution to surface O_3 (O_3P). O_3P reached a maximum of 15% at 00:00 BJT on July 17. By analyzing the weather condition in Section 3.2, we found that the strongest upper-air trough occurred over Jiangsu, while the simulated maximum stratospheric contribution occurred over Shandong. This discrepancy may be partly explained by the difference in terrain height. In provinces with greater elevations, such as Shandong, Henan, and Hubei, stratospheric O_3 was more easily able to reach the ground (Figure 1A).

3.4 Contribution of different processes to O₃ variation during stratospheric intrusion

To quantify the contribution of different process on surface O_3, IPR analysis is utilized in this section. We selected four grid points over Jiangsu province, where the impact of the intrusion is significant (Figure 8E). The time span used to calculate the contribution of each process is 6 h. Figure 8 depicts the vertical profile of the ADVZ contribution during the intrusion. A clear positive contribution of up to 12.9 ppb h^{-1} is found in the upper troposphere over Xuzhou and extends down to about 13 km (grid point a). Further to the southeast, the peak of the positive ADVZ contribution gradually appears at the lower position of the free troposphere. For example, at grid point b (near Suqian), the maximum contribution is about 9.9 ppb h^{-1} at 8 km, and the positive contribution extends from 12 km to 8 km, while grid point c (near Huaian) indicates the maximum positive contribution of about 15 ppb h^{-1} at 6 km, and the positive contribution extends down to near 2 km. Further downstream, grid point d (near Yancheng) shows a positive contribution of about 10.15 ppb h^{-1} near 2.5 km. This provides evidence that O_3 is transported vertically towards the surface from the northwest to the southeast. Although we analyzed only one transport route, similar transport paths (northwest-southeast) occurred through the Jiangsu and Shandong provinces during the SI.

Figure 9 shows the mean contributions of different physical/chemical processes to O_3 concentration at the four grid points during SI. As shown in Figure 9A, the contributions from photochemical production were negligible in the free troposphere, where O_3 precursors of nitrogen oxides and volatile organic compounds are limited. The ADV dominated the NET variation in O_3, with positive contributions ranging from 0.1 to 13.8 ppb h^{-1}. The contribution of ADV reduces as altitude decrease due to a gradual weakening of intrusion intensity. Undoubtedly, the contribution of ADV to O_3 in the free troposphere was attributed to SI. To further quantify the influence of SI on near-surface O_3, we analyzed the contribution of ADVZ and ADVH to O_3 within the planetary boundary layer (Figure 9B). We suggested that during a SI, O_3 from the stratosphere does not reach the surface directly but is first transported vertically to the boundary layer and then influenced downwind areas by horizontal advection. During this intrusion event, ADVH was the dominant process contributing to the increase in near-surface O_3 (from 30 to 690 m), with values being 1.7–13.5 ppb h^{-1}.

4 Conclusion

In this study, we simulated a typical SI event that occurred over eastern China from 15 to 19 July 2016 using the regional model WRF-Chem and examined the impacts of SI on surface O_3 pollution. The results indicate that the large-scale circulation pattern during SI was characterized by a deep trough over central-to-North China, the South Asia high and the Western Pacific subtropical high. The downdrafts in the west of the upper-level trough carried O_3-rich stratospheric air into the troposphere when the deep trough passed across eastern China. The spatial distribution and longitude-pressure cross-section of O_3 at 300 hPa revealed a significant increase in O_3 over eastern China during SI. Using a tracer tagging technique, we quantified the contribution of SI to surface O_3 concentrations of up to 6.5 ppb. The IPR analysis was used to quantify the contribution of different physical/chemical processes to O_3 variations during SI. The results

indicate that the ADV dominated the NET variation in free troposphere O_3, with positive contribution ranging from 0.1 to 13.8 ppb h^{-1}. The contribution of ADV reduces as altitude decreases due to a gradual weakening of intrusion intensity. ADVH was the dominant contributor to the increase in near-surface O_3 (from 30 to 690 m), with values ranging between 1.7 and 13.5 ppb h^{-1}. O_3 from SI reached the near surface and then influenced a larger area through horizontal advection.

SI as a natural factor makes O_3 pollution mitigation more challenging. We argue that, while strictly regulating anthropogenic emissions, we should strengthen the identification of SI and develop discriminating criteria to detect its occurrence.

Data availability statement

The raw data supporting the conclusion of this article will be made available by the authors, without undue reservation.

Author contributions

Data curation, model simulation, visualization and writing-original draft preparation, FC; Supervision, funding acquisition, writing-review and editing, NL, JL, and HL All authors have read and agreed to the published version of the manuscript.

Conflict of interest

The authors declare that the research was conducted in the absence of any commercial or financial relationships that could be construed as a potential conflict of interest.

Publisher's note

All claims expressed in this article are solely those of the authors and do not necessarily represent those of their affiliated organizations, or those of the publisher, the editors and the reviewers. Any product that may be evaluated in this article, or claim that may be made by its manufacturer, is not guaranteed or endorsed by the publisher.

References

Abdallah, C., Sartelet, K., and Afif, C. (2016). Influence of boundary conditions and anthropogenic emission inventories on simulated O 3 and PM 2.5 concentrations over Lebanon. *Atmos. Pollut. Res.* 7 (6), 971–979. doi:10.1016/j.apr.2016.06.001

Akritidis, D., Pozzer, A., Zanis, P., Tyrlis, E., Škerlak, B., Sprenger, M., et al. (2016). On the role of tropopause folds in summertime tropospheric ozone over the eastern Mediterranean and the Middle East. *Atmos. Chem. Phys.* 16 (21), 14025–14039. doi:10.5194/acp-16-14025-2016

Asuero, A. G., Sayago, A., and González, A. G. (2007). The correlation coefficient: An overview. *Crit. Rev. Anal. Chem.* 36 (1), 41–59. doi:10.1080/10408340500526766

Barth, M. C., Lee, J., Hodzic, A., Pfister, G., Skamarock, W. C., Worden, J., et al. (2012). Thunderstorms and upper troposphere chemistry during the early stages of the 2006 North American Monsoon. *Atmos. Chem. Phys.* 12 (22), 11003–11026. doi:10.5194/acp-12-11003-2012

Carter, L, W. P. (2000). "Documentation of the SAPRC-99 chemical mechanism for VOC reactivity assessment," in Report to the California air resources board*)*, 95–308.

Chen, D., Zhou, T., Guo, D., and Ge, S. (2021). Simulation of the multi-timescale stratospheric intrusion processes in a typical cut-off low over northeast Asia. *Atmosphere* 13 (1), 68. doi:10.3390/atmos13010068

Chen, L., Zhu, J., Liao, H., Gao, Y., Qiu, Y., Zhang, M., et al. (2019). Assessing the formation and evolution mechanisms of severe haze pollution in the Beijing–Tianjin–Hebei region using process analysis. *Atmos. Chem. Phys.* 19 (16), 10845–10864. doi:10.5194/acp-19-10845-2019

Dai, H., Zhu, J., Liao, H., Li, J., Liang, M., Yang, Y., et al. (2021). Co-occurrence of ozone and PM2.5 pollution in the Yangtze River Delta over 2013–2019: Spatiotemporal distribution and meteorological conditions. *Atmos. Res.* 249, 105363. doi:10.1016/j.atmosres.2020.105363

Dang, R., Liao, H., and Fu, Y. (2021). Quantifying the anthropogenic and meteorological influences on summertime surface ozone in China over 2012-2017. *Sci. Total Environ.* 754, 142394. doi:10.1016/j.scitotenv.2020.142394

Dang, R., and Liao, H. (2019). Radiative forcing and health impact of aerosols and ozone in China as the consequence of clean air actions over 2012–2017. *Geophys. Res. Lett.* 46 (21), 12511–12519. doi:10.1029/2019GL084605

Davies, T. D., and Schuepbach, E. (1994). Episodes of high ozone concentrations at the earth's surface resulting from transport down from the upper troposphere/lower stratosphere: A review and case studies. *Atmos. Environ.* 28 (1), 53–68. doi:10.1016/1352-2310(94)90022-1

Emmons, L. K., Lamarque, J.-F., Granier, C., Guenther, A., et al. (2010). Description and evaluation of the model for ozone and related chemical tracers, version 4 (MOZART-4). *Geosci. Model. Dev.* 3, 43–67. doi:10.5194/gmd-3-43-2010

Finlayson-Pitts, B. J., and Pitts, J. N. (1997). Tropospheric air pollution: Ozone, airborne toxics, polycyclic aromatic hydrocarbons, and particles. *Science* 276 (5315), 1045–1051. doi:10.1126/science.276.5315.1045

Fleming, Z. L., Doherty, R. M., von Schneidemesser, E., Malley, C. S., Cooper, O. R., Pinto, J. P., et al. (2018). Tropospheric Ozone Assessment Report: Present-day ozone distribution and trends relevant to human health. *Elementa-Science Of Anthropocene* 6. doi:10.1525/elementa.273

Ganguly, N. D. (2012). Influence of stratospheric intrusion on the surface ozone levels in India. *ISRN Meteorol.* 2012, 1–7. doi:10.5402/2012/625318

Gao, J., Zhu, B., Xiao, H., Kang, H., Hou, X., and Shao, P. (2016). A case study of surface ozone source apportionment during a high concentration episode, under frequent shifting wind conditions over the Yangtze River Delta, China. *Sci. Total Environ.* 544, 853–863. doi:10.1016/j.scitotenv.2015.12.039

Gao, J., Zhu, B., Xiao, H., Kang, H., Pan, C., Wang, D., et al. (2018). Effects of black carbon and boundary layer interaction on surface ozone in Nanjing, China. *Atmos. Chem. Phys.* 18 (10), 7081–7094. doi:10.5194/acp-18-7081-2018

Gonçalves, M., Jiménez-Guerrero, P., and Baldasano, J. M. (2009). Contribution of atmospheric processes affecting the dynamics of air pollution in South-Western Europe during a typical summertime photochemical episode. *Atmos. Chem. Phys.* 9 (3), 849–864. doi:10.5194/acp-9-849-2009

Gong, C., Liao, H., Zhang, L., Yue, X., Dang, R., and Yang, Y. (2020). Persistent ozone pollution episodes in North China exacerbated by regional transport. *Environ. Pollut.* 265, 115056. doi:10.1016/j.envpol.2020.115056

Greenslade, J. W., Alexander, S. P., Schofield, R., Fisher, J. A., and Klekociuk, A. K. (2017). Stratospheric ozone intrusion events and their impacts on tropospheric ozone in the Southern Hemisphere. *Atmos. Chem. Phys.* 17 (17), 10269–10290. doi:10.5194/acp-17-10269-2017

Grell, G. A., Peckham, S. E., Schmitz, R., McKeen, S. A., Frost, G., Skamarock, W. C., et al. (2005). Fully coupled "online" chemistry within the WRF model. *Atmos. Environ.* 39 (37), 6957–6975. doi:10.1016/j.atmosenv.2005.04.027

Guenther, A., Harley, P., Wiedinmyer, C., Palmer, P. I., and Geron, C. (2006). Estimates of global terrestrial isoprene emissions using MEGAN (model of emissions of Gases and aerosols from nature). *Atmos. Chem. Phys.* 6, 3181–3210. doi:10.5194/acp-6-3181-2006

Hocking, W. K., Carey-Smith, T., Tarasick, D. W., Argall, P. S., Strong, K, Rochon, Y., et al. (2007). Detection of stratospheric ozone intrusions by windprofiler radars. *Nature* 450 (7167), 281–284. doi:10.1038/nature06312

Holton, J. R., Haynes, H., Mclntyre, P., R., Douglass, M., R., Rood, B. R., and Pfister, L. (1995). Stratosphere-troposphere exchange. *Rev. Geophys.* 33 (4), 403–439. doi:10.1029/95rg02097

Huang, S., Huang, P.-R., Newman, S., Li, K.-F., Lin, Y.-C., Huh, C.-A., et al. (2022). Enhanced stratospheric intrusion at Lulin Mountain, Taiwan inferred from beryllium-7 activity. *Atmos. Environ.* 268, 118824. doi:10.1016/j.atmosenv.2021.118824

Jr, W. I. G., and Yu, S. (2012). Generalized approach for using unbiased symmetric metrics with negative values: Normalized mean bias factor and normalized mean absolute error factor. *Atmos. Sci. Lett.* 13 (4), 262–267. doi:10.1002/asl.393

Karlický, J., Huszár, P., and Halenka, T. (2017). Validation of gas phase chemistry in the WRF-Chem model over Europe. *Adv. Sci. Res.* 14, 181–186. doi:10.5194/asr-14-181-2017

Knowland, K. E., Ott, L. E., Duncan, B. N., and Wargan, K. (2017). Stratospheric intrusion-influenced ozone air quality exceedances investigated in the NASA MERRA-2 Reanalysis. *Geophys Res. Lett.* 44 (20), 10691–10701. doi:10.1002/2017gl074532

Lamarque, J. F., Emmons, L. K., Hess, P. G., Kinnison, D. E., Tilmes, S., Vitt, F., et al. (2012). CAM-Chem: Description and evaluation of interactive atmospheric chemistry in the community earth system model. *Geosci. Model. Dev.* 5 (2), 369–411. doi:10.5194/gmd-5-369-2012

Langford, A. O., Masters, C. D., Proffitt, M. H., Hsie, E.-Y., and Tuck, A. F. (1996). Ozone measurements in a tropopause fold associated with a cut-off low system. *Geophys. Res. Lett.* 23 (18), 2501–2504. doi:10.1029/96GL02227

Lelieveld, J., Evans, J. S., Fnais, M., Giannadaki, D., and Pozzer, A. (2015). The contribution of outdoor air pollution sources to premature mortality on a global scale. *Nature* 525 (7569), 367–371. doi:10.1038/nature15371

Li, D., Bian, J., and Fan, Q. (2015). A deep stratospheric intrusion associated with an intense cut-off low event over East Asia. *Sci. China Earth Sci.* 58 (1), 116–128. doi:10.1007/s11430-014-4977-2

Li, K., Jacob, D. J., Liao, H., Shen, L., Zhang, Q., and Bates, K. H. (2019a). Anthropogenic drivers of 2013-2017 trends in summer surface ozone in China. *PNAS* 116 (2), 422–427. doi:10.1073/pnas.1812168116

Li, K., Jacob, D. J., Liao, H., Zhu, J., Shah, V., Shen, L., et al. (2019b). A two-pollutant strategy for improving ozone and particulate air quality in China. *Nat. Geosci.* 12 (11), 906–910. doi:10.1038/s41561-019-0464-x

Li, K., Jacob, D. J., Shen, L., Lu, X., De Smedt, I., and Liao, H. (2020). Increases in surface ozone pollution in China from 2013 to 2019: Anthropogenic and meteorological influences. *Atmos. Chem. Phys.* 20 (19), 11423–11433. doi:10.5194/acp-20-11423-2020

Li, M, Zhang, Q., Kurokawa, J.-i., Woo, J.-H., He, K., Lu, Z., et al. (2017). Mix: A mosaic asian anthropogenic emission inventory under the international collaboration framework of the MICS-asia and HTAP. *Atmos. Chem. Phys.* 17 (2), 935–963. doi:10.5194/acp-17-935-2017

Lin, M., Fiore, A. M., Horowitz, L. W., Langford, A. O., Oltmans, S. J., Tarasick, D., et al. (2015). Climate variability modulates Western US ozone air quality in spring via deep stratospheric intrusions. *Nat. Commun.* 6, 7105. doi:10.1038/ncomms8105

Meng, K., Zhao, T., Xu, X., Zhang, Z., Bai, Y., Hu, Y., et al. (2022). Influence of stratosphere-to-troposphere transport on summertime surface O3 changes in North China Plain in 2019. *Atmos. Res.* 276, 106271. doi:10.1016/j.atmosres.2022.106271

Mills, G., Sharps, K., Simpson, D., Pleijel, H., Broberg, M., Uddling, J., et al. (2018). Ozone pollution will compromise efforts to increase global wheat production. *Glob. Change Biol.* 24 (8), 3560–3574. doi:10.1111/gcb.14157

Ni, Z.-Z., Luo, K., Gao, X., Gao, Y., Fan, J.-R., Fu, J. S., et al. (2019). Exploring the stratospheric source of ozone pollution over China during the 2016 Group of Twenty summit. *Atmos. Pollut. Res.* 10 (4), 1267–1275. doi:10.1016/j.apr.2019.02.010

Nieto, R., Gimeno, L., de la Torre, L., Ribera, P., Gallego, D., García-Herrera, R., et al. (2005). Climatological features of cutoff low systems in the northern hemisphere. *J. Clim.* 18 (16), 3085–3103. doi:10.1175/jcli3386.1

Ou-Yang, H., Chen, L., Liao, H., Zhu, J., Wang, W., and Li, X. (2022). Impacts of aerosol–photolysis interaction and aerosol–radiation feedback on surface-layer ozone in North China during multi-pollutant air pollution episodes. *Atmos. Chem. Phys.* 22 (6), 4101–4116. doi:10.5194/acp-22-4101-2022

Qian, J., Liao, H., Yang, Y., Li, K., Chen, L., and Zhu, J. (2022). Meteorological influences on daily variation and trend of summertime surface ozone over years of 2015-2020: Quantification for cities in the Yangtze River Delta. *Sci. Total Environ.* 834, 155107. doi:10.1016/j.scitotenv.2022.155107

Stohl, A., Bonasoni, P., Cristofanelli, P., Collins, W., Feichter, J., Frank, A., et al. (2003a). Stratosphere-troposphere exchange: A review, and what we have learned from staccato. *J. Geophys. Res. Atmos.* 108 (D12), 8516. doi:10.1029/2002JD002490

Stohl, A., Bonasoni, P., Cristofanelli, P., Collins, W., Feichter, J., Frank, A., et al. (2003b). Stratosphere-troposphere exchange: A review, and what we have learned from staccato. *J. Geophys. Res.* 108 (D12), 8516. doi:10.1029/2002jd002490

Tang, K., Zhang, H., Feng, W., Liao, H., Hu, J., and Li, N. (2022). Increasing but variable trend of surface ozone in the yangtze river delta region of China. *Front. Environ. Sci.* 10. doi:10.3389/fenvs.2022.836191

Wang, H., Wang, W., Huang, X., and Ding, A. (2020a). Impacts of stratosphere-to-troposphere-transport on summertime surface ozone over eastern China. *Sci. Bull.* 65 (4), 276–279. doi:10.1016/j.scib.2019.11.017

Wang, T., Xue, L., Brimblecombe, P., Lam, Y. F., Li, L., and Zhang, L. (2017). Ozone pollution in China: A review of concentrations, meteorological influences, chemical precursors, and effects. *Sci. Total Environ.* 575, 1582–1596. doi:10.1016/j.scitotenv.2016.10.081

Wang, X., Wu, Y., Randel, W., and Tilmes, S. (2020b). Stratospheric contribution to the summertime high surface ozone events over the Western United States. *Environ. Res. Lett.* 15 (10), 1040a6. doi:10.1088/1748-9326/abba53

Wiedinmyer, C., Akagi, S. K., Yokelson, R. J., Emmons, L. K., Al-Saadi, J. A., Orlando, J. J., et al. (2011). The Fire INventory from NCAR (FINN): A high resolution global model to estimate the emissions from open burning. *Geosci. Model. Dev.* 4 (3), 625–641. doi:10.5194/gmd-4-625-2011

Xu, X., Lin, W., Xu, W., Jin, J., Wang, Y., Zhang, G., et al. (2020). Long-term changes of regional ozone in China: Implications for human health and ecosystem impacts. *Elementa-Science Of Anthropocene* 8. doi:10.1525/elementa.409

Yahya, K., Wang, K., Gudoshava, M., Glotfelty, T., and Zhang, Y. (2015). Application of WRF/chem over North America under the AQMEII phase 2: Part I. Comprehensive evaluation of 2006 simulation. *Atmos. Environ.* 115, 733–755. doi:10.1016/j.atmosenv.2014.08.063

Žabkar, R., Rakovec, J., and Koračin, D. (2011). The roles of regional accumulation and advection of ozone during high ozone episodes in Slovenia: A WRF/chem modelling study. *Atmos. Environ.* 45 (5), 1192–1202. doi:10.1016/j.atmosenv.2010.08.021

Zaveri, R. A., Easter, R. C., Fast, J. D., and Peters, L. K. (2008). Model for simulating aerosol Interactions and chemistry (MOSAIC). *J. Geophys. Res.* 113 (D13), D13204. doi:10.1029/2007jd008782

Zhai, S., Jacob, D. J., Wang, X., Shen, L., Li, K., Zhang, Y., et al. (2019). Fine particulate matter ($PM_{2.5}$) trends in China, 2013–2018: Separating contributions from anthropogenic emissions and meteorology. *Atmos. Chem. Phys.* 19 (16), 11031–11041. doi:10.5194/acp-19-11031-2019

Zhang, B., Wang, Y., and Hao, J. (2015). Simulating aerosol–radiation–cloud feedbacks on meteorology and air quality over eastern China under severe haze conditionsin winter. *Atmos. Chem. Phys.* 15 (5), 2387–2404. doi:10.5194/acp-15-2387-2015

Zhang, Y., Li, J., Yang, W., Du, H., Tang, X., Ye, Q., et al. (2022). Influences of stratospheric intrusions to high summer surface ozone over a heavily industrialized region in northern China. *Environ. Res. Lett.* 17 (9), 094023. doi:10.1088/1748-9326/ac8b24

Zhao, K., Hu, C., Yuan, Z., Xu, D., Zhang, S., Luo, H., et al. (2021a). A modeling study of the impact of stratospheric intrusion on ozone enhancement in the lower troposphere over the Hong Kong regions, China. *Atmos. Res.* 247, 105158. doi:10.1016/j.atmosres.2020.105158

Zhao, K., Huang, J., Wu, Y., Yuan, Z., Wang, Y., Li, Y., et al. (2021b). Impact of stratospheric intrusions on ozone enhancement in the lower troposphere and implication to air quality in Hong Kong and other South China regions. *J. Geophys. Res. Atmos.* 126 (18). doi:10.1029/2020jd033955